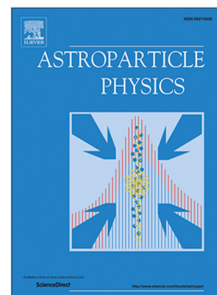


Journal Pre-proof

Study of cosmogenic activation above ground for the DarkSide-20k experiment



E. Aaron, P. Agnes, I. Ahmad, S. Albergo, I.F.M. Albuquerque,
T. Alexander, A.K. Alton, P. Amaudruz, M. Atzori Corona, M. Ave,
I.Ch. Avetisov, O. Azzolini, H.O. Back, Z. Balmforth,
A. Barrado-Olmedo, P. Barrillon, A. Basco, G. Batignani, V. Bocci,
W.M. Bonivento, B. Bottino, M.G. Boulay, J. Bustos, M. Cadeddu,
A. Caminata, N. Canci, A. Capra, S. Caprioli, M. Caravati, N. Cargioli,
M. Carlini, P. Castello, P. Cavalcante, S. Cavuoti, S. Cebrian, J.M. Cela
Ruiz, S. Chashin, A. Chepurnov, E. Chyhrynets, L. Cifarelli,
D. Cintas, M. Citterio, B. Cleveland, V. Cocco, D. Colaiuda, E. Conde
Vilda, L. Consiglio, S. Copello, G. Covone, M. Czubak, M. D'Aniello,
S. D'Auria, M.D. Da Rocha Rolo, S. Davini, S. De Cecco, D. De
Gruttola, S. De Pasquale, G. De Rosa, G. Dellacasa, A.V. Derbin,
A. Devoto, F. Di Capua, L. Di Noto, P. Di Stefano, G. Dolganov,
F. Dordei, E. Ellingwood, T. Erjavec, M. Fernandez Diaz, G. Fiorillo,
P. Franchini, D. Franco, N. Funicello, F. Gabriele, D. Gahan,
C. Galbiati, G. Gallina, G. Gallus, M. Garbini, P. Garcia Abia,
A. Gendotti, C. Ghiano, C. Giganti, G.K. Giovanetti, V. Goicoechea
Casanueva, A. Gola, G. Grauso, G. Grilli di Cortona, A. Grobov,
M. Gromov, M. Guan, M. Guerzoni, M. Gulino, C. Guo, B.R. Hackett,
A.L. Hallin, A. Hamer, M. Haranczyk, T. Hessel, S. Hill, S. Horikawa,
F. Hubaut, J. Hucker, T. Hugues, A. Ianni, V. Ippolito, C. Jillings,
S. Jois, P. Kachru, A.A. Kemp, C.L. Kendziora, M. Kimura,
I. Kochanek, K. Kondo, G. Korga, S. Koulosousas, A. Kubankin,
M. Kuss, M. Kuzniak, M. La Commara, M. Lai, E. Le Guirriec,
E. Leason, A. Leoni, L. Lidey, M. Lissia, L. Luzzi, O. Lychagina,
O. Macfadyen, I.N. Machulin, S. Manecki, I. Manthos, L. Mapelli,
A. Margotti, S.M. Mari, C. Mariani, J. Maricic, A. Marini,
M. Martínez, C.J. Martoff, G. Matteucci, K. Mavrokoridis,
A.B. McDonald, A. Messina, R. Milincic, A. Mitra, A. Moharana,
J. Monroe, E. Moretti, M. Morrocchi, T. Mróz, V.N. Muratova,
C. Muscas, P. Musico, R. Nania, M. Nessi, G. Nieradka,
K. Nikolopoulos, J. Nowak, K. Olchansky, A. Oleinik, V. Oleynikov,
P. Organini, A. Ortiz de Solórzano, L. Pagani, M. Pallavicini,
L. Pandola, E. Pantic, E. Paoloni, G. Paternoster, P.A. Pegoraro,
K. Pelczar, C. Pellegrino, V. Pesudo, S. Piacentini, L. Pietrofaccia,
N. Pino, A. Pocar, D.M. Poehlmann, S. Pordes, P. Pralavorio, D. Price,
F. Ragusa, Y. Ramachers, M. Razeti, A.L. Renshaw, M. Rescigno,
F. Retiere, L.P. Rignanese, C. Ripoli, A. Rivetti, A. Roberts,
C. Roberts, J. Rode, G. Rogers, L. Romero, M. Rossi, A. Rubbia,
M.A. Sabia, P. Salomone, E. Sandford, S. Sanfilippo, D. Santone,
R. Santorelli, C. Savarese, E. Scapparone, G. Schillaci,
F.G. Schuckman II, G. Scioli, M. Simeone, P. Skensved,
M.D. Skorokhvatov, O. Smirnov, T. Smirnova, B. Smith, F. Spadoni,

M. Spangenberg, R. Stefanizzi, A. Steri, V. Stornelli, S. Stracka,
M. Stringer, S. Sulis, A. Sung, Y. Suvorov, A.M. Szelc, R. Tartaglia,
A. Taylor, J. Taylor, S. Tedesco, G. Testera, K. Thieme, T.N. Thorpe,
A. Tonazzo, A. Tricomi, E.V. Unzhakov, T. Vallivilayil John, M. Van
Uffelen, T. Viant, S. Viel, R.B. Vogelaar, J. Vossebeld, M. Wada,
M.B. Walczak, H. Wang, Y. Wang, S. Westerdale, L. Williams,
I. Wingerter-Seez, R. Wojaczynski, Ma.M. Wojcik, T. Wright, Y. Xie,
C. Yang, A. Zabihi, P. Zakhary, A. Zani, A. Zichichi, G. Zuzel,
M.P. Zykova, The DarkSide-20k Collaboration

PII: S0927-6505(23)00064-6
DOI: <https://doi.org/10.1016/j.astropartphys.2023.102878>
Reference: ASTPHY 102878

To appear in: *Astroparticle Physics*

Received date: 30 January 2023

Revised date: 22 June 2023

Accepted date: 23 June 2023

Please cite this article as: E. Aaron, P. Agnes, I. Ahmad et al., Study of cosmogenic activation above ground for the DarkSide-20k experiment, *Astroparticle Physics* (2023), doi: <https://doi.org/10.1016/j.astropartphys.2023.102878>.

This is a PDF file of an article that has undergone enhancements after acceptance, such as the addition of a cover page and metadata, and formatting for readability, but it is not yet the definitive version of record. This version will undergo additional copyediting, typesetting and review before it is published in its final form, but we are providing this version to give early visibility of the article. Please note that, during the production process, errors may be discovered which could affect the content, and all legal disclaimers that apply to the journal pertain.

© 2023 Published by Elsevier B.V.

Study of cosmogenic activation above ground for the DarkSide-20k experiment

E. Aaron^a, P. Agnes^b, I. Ahmad^c, S. Albergo^{d,e}, I. F. M. Albuquerque^f, T. Alexander^g, A. K. Alton^h, P. Amaudruzⁱ, M. Atzori Corona^j, M. Ave^f, I. Ch. Avetisov^k, O. Azzolini^l, H. O. Back^g, Z. Balmforth^m, A. Barrado-Olmedoⁿ, P. Barrillon^o, A. Basco^p, G. Batignani^{q,r}, V. Bocci^s, W. M. Bonivento^j, B. Bottino^{t,u,v}, M. G. Boulay^w, J. Bustos^o, M. Cadeddu^j, A. Caminata^u, N. Canci^p, A. Capraⁱ, S. Caprioli^{t,u}, M. Caravati^j, N. Cargioli^{x,j}, M. Carlini^y, P. Castello^{z,j}, P. Cavalcante^y, S. Cavuoti^{aa,p}, S. Cebrian^{ab}, J. M. Cela Ruizⁿ, S. Chashin^{ac}, A. Chepurnov^{ac}, E. Chyhyrynets^l, L. Cifarelli^{ad,ae}, D. Cintas^{ab}, M. Citterio^{af}, B. Cleveland^{ag,ah}, V. Cocco^j, D. Colaiuda^{ai,y}, E. Conde Vildaⁿ, L. Consiglio^y, S. Copello^{u,t}, G. Covone^{aa,p}, M. Czubak^{aj}, M. D'Aniello^{ak,p}, S. D'Auria^{af}, M. D. Da Rocha Rolo^{al}, S. Davini^u, S. De Cecco^{s,am}, D. De Gruttola^{an,ao}, S. De Pasquale^{an,ao}, G. De Rosa^{aa,p}, G. Dellacasa^{al}, A. V. Derbin^{ap}, A. Devoto^{x,j}, F. Di Capua^{aa,p}, L. Di Noto^{t,u}, P. Di Stefano^{aq}, G. Dolganov^{ar}, F. Dordei^j, E. Ellingwood^{aq}, T. Erjavec^a, M. Fernandez Diazⁿ, G. Fiorillo^{aa,p}, P. Franchini^{as,m}, D. Franco^{at}, N. Funicello^{an,ao}, F. Gabriele^j, D. Gahan^{x,j}, C. Galbiati^{v,y,b}, G. Gallina^v, G. Gallus^j, M. Garbini^{au,ae,ad}, P. Garcia Abiaⁿ, A. Gendotti^{av}, C. Ghiano^y, C. Giganti^{aw}, G. K. Giovanetti^{ax}, V. Goicoechea Casanueva^{ay}, A. Gola^{az,ba}, G. Graus^P, G. Grilli di Cortona^s, A. Grobov^{ar,bb}, M. Gromov^{ac,bc}, M. Guan^{bd}, M. Guerzoni^{ae}, M. Gulino^{be,bf}, C. Guo^{bd}, B. R. Hackett^g, A. L. Hallin^{bg}, A. Hamer^{bh,m}, M. Haranczyk^{aj}, T. Hessel^{at}, S. Hill^m, S. Horikawa^{ai,y}, F. Hubaut^o, J. Hucker^{aq}, T. Hugues^c, An. Ianni^{v,y}, V. Ippolito^s, C. Jillings^{ag,ah}, S. Jois^m, P. Kachru^{b,y}, A. A. Kemp^{aq}, C. L. Kendziora^{bi}, M. Kimura^c, I. Kochanek^y, K. Kondo^{ai,y}, G. Korga^m, S. Koulosousas^m, A. Kubankin^{bj}, M. Kuss^q, M. Kuzniak^c, M. La Commara^{bk,p}, M. Lai^{x,j}, E. Le Guirriec^o, E. Leason^m, A. Leoni^{ai,y}, L. Lidey^g, M. Lissia^j, L. Luzziⁿ, O. Lychagina^{bc}, O. Macfadyen^m, I. N. Machulin^{ar,bb}, S. Manecki^{ag,ah}, I. Manthos^{bl}, L. Mapelli^v, A. Margotti^{ae}, S. M. Mari^{bm,bn}, C. Mariani^{bo}, J. Maricic^{ay}, A. Marini^{t,u}, M. Martínez^{ab,bp}, C. J. Martoff^{bq}, G. Matteucci^p, K. Mavrokordidis^{br}, A. B. McDonald^{aq}, A. Messina^{s,am}, R. Milincic^{ay}, A. Mitra^{bs}, A. Moharana^{b,y}, J. Monroe^m, E. Moretti^{az,ba}, M. Morrocchi^{q,r}, T. Mróz^{aj}, V. N. Muratova^{ap}, C. Muscas^{z,j}, P. Musico^u, R. Nania^{ae}, M. Nessi^y,

G. Nieradka^c, K. Nikolopoulos^{bl}, J. Nowak^{as}, K. Olchanskyⁱ, A. Oleinik^{bj},
 V. Oleynikov^{bt,bu}, P. Organini^v, A. Ortiz de Solórzano^{ab}, L. Pagani^a,
 M. Pallavicini^{t,u}, L. Pandola^{bf}, E. Pantic^a, E. Paoloni^{q,r}, G. Paternoster^{az,ba},
 P. A. Pegoraro^{z,j}, K. Pelczar^{aj}, C. Pellegrino^{ae}, V. Pesudoⁿ,
 S. Piacentini^{am,s}, L. Pietrofaccia^y, N. Pino^{d,e}, A. Pocar^{bv},
 D. M. Poehlmann^a, S. Pordes^{bi}, P. Pralavorio^o, D. Price^{bw}, F. Ragusa^{bx,af},
 Y. Ramachers^{bs}, M. Razeti^j, A. L. Renshaw^{by}, M. Rescigno^s, F. Retiereⁱ,
 L. P. Rignanese^{ae,ad}, C. Ripoli^{ao,an}, A. Rivetti^{al}, A. Roberts^{br}, C. Roberts^{bw},
 J. Rode^{aw,at}, G. Rogers^{bl}, L. Romeroⁿ, M. Rossi^{u,t}, A. Rubbia^{av},
 M. A. Sabia^{s,am}, P. Salomone^{s,am}, E. Sandford^{bw}, S. Sanfilippo^{bf},
 D. Santone^m, R. Santorelliⁿ, C. Savarese^v, E. Scapparone^{ae}, G. Schillaci^{bf},
 F. G. Schuckman II^{aq}, G. Scioli^{ad,ae}, M. Simeone^{bz,p}, P. Skensved^{aq},
 M. D. Skorokhvatov^{ar,bb}, O. Smirnov^{bc}, T. Smirnova^{ar}, B. Smithⁱ,
 F. Spadoni^g, M. Spangenberg^{bs}, R. Stefanizzi^{x,j}, A. Steri^j, V. Stornelli^{ai,y},
 S. Stracka^q, M. Stringer^{aq}, S. Sulis^{z,j}, A. Sung^v, Y. Suvorov^{aa,p,ar},
 A. M. Szelc^{bh}, R. Tartaglia^y, A. Taylor^{br}, J. Taylor^{br}, S. Tedesco^{ca},
 G. Testera^u, K. Thieme^{ay}, T. N. Thorpe^{cb}, A. Tonazzo^{at}, A. Tricomi^{d,e},
 E. V. Unzhakov^{ap}, T. Vallivilayil John^{b,y}, M. Van Uffelen^o, T. Viant^{av},
 S. Viel^w, R. B. Vogelaar^{bo}, J. Vossebeld^{br}, M. Wada^{c,x}, M. B. Walczak^c,
 H. Wang^{cb}, Y. Wang^{bd,cc}, S. Westerdale^{cd}, L. Williams^{ce},
 I. Wingerter-Seez^o, R. Wojaczynski^c, Ma. M. Wojeik^{aj}, T. Wright^{bo},
 Y. Xie^{bd,cc}, C. Yang^{bd,cc}, A. Zabihi^c, P. Zakhary^c, A. Zani^{af}, A. Zichichi^{ad,ae},
 G. Zuzel^{aj}, M. P. Zyкова^k, (The DarkSide-20k Collaboration)¹

^aDepartment of Physics, University of California, Davis, CA 95616, USA

^bGran Sasso Science Institute, L'Aquila 67100, Italy

^cAstroCeNT, Nicolaus Copernicus Astronomical Center of the Polish Academy of Sciences, 00-614 Warsaw, Poland

^dINFN Catania, Catania 95121, Italy

^eUniversità di Catania, Catania 95124, Italy

^fInstituto de Física, Universidade de São Paulo, São Paulo 05508-090, Brazil

^gPacific Northwest National Laboratory, Richland, WA 99352, USA

^hPhysics Department, Augustana University, Sioux Falls, SD 57197, USA

ⁱTRIUMF, 4004 Wesbrook Mall, Vancouver, BC V6T 2A3, Canada

^jINFN Cagliari, Cagliari 09042, Italy

^kMendeleev University of Chemical Technology, Moscow 125047, Russia

^lINFN Laboratori Nazionali di Legnaro, Legnaro (Padova) 35020, Italy

^mDepartment of Physics, Royal Holloway University of London, Egham TW20 0EX, UK

¹e-mail: ds-ed@lngs.infn.it

ⁿ*CIEMAT, Centro de Investigaciones Energéticas, Medioambientales y Tecnológicas, Madrid 28040, Spain*

^o*Centre de Physique des Particules de Marseille, Aix Marseille Univ, CNRS/IN2P3, CPPM, Marseille, France*

^p*INFN Napoli, Napoli 80126, Italy*

^q*INFN Pisa, Pisa 56127, Italy*

^r*Physics Department, Università degli Studi di Pisa, Pisa 56127, Italy*

^s*INFN Sezione di Roma, Roma 00185, Italy*

^t*Physics Department, Università degli Studi di Genova, Genova 16146, Italy*

^u*INFN Genova, Genova 16146, Italy*

^v*Physics Department, Princeton University, Princeton, NJ 08544, USA*

^w*Department of Physics, Carleton University, Ottawa, ON K1S 5B6, Canada*

^x*Physics Department, Università degli Studi di Cagliari, Cagliari 09042, Italy*

^y*INFN Laboratori Nazionali del Gran Sasso, Assergi (AQ) 67100, Italy*

^z*Department of Electrical and Electronic Engineering, Università degli Studi di Cagliari, Cagliari 09123, Italy*

^{aa}*Physics Department, Università degli Studi "Federico II" di Napoli, Napoli 80126, Italy*

^{ab}*Centro de Astropartículas y Física de Altas Energías, Universidad de Zaragoza, Zaragoza 50009, Spain*

^{ac}*Skobeltsyn Institute of Nuclear Physics, Lomonosov Moscow State University, Moscow 119234, Russia*

^{ad}*Department of Physics and Astronomy, Università degli Studi di Bologna, Bologna 40126, Italy*

^{ae}*INFN Bologna, Bologna 40126, Italy*

^{af}*INFN Milano, Milano 20133, Italy*

^{ag}*SNOLAB, Lively, ON P3Y 1N2, Canada*

^{ah}*Department of Physics and Astronomy, Laurentian University, Sudbury, ON P3E 2C6, Canada*

^{ai}*Università degli Studi dell'Aquila, L'Aquila 67100, Italy*

^{aj}*M. Smoluchowski Institute of Physics, Jagiellonian University, 30-348 Krakow, Poland*

^{ak}*Department of Strutture per l'Ingegneria e l'Architettura, Università degli Studi "Federico II" di Napoli, Napoli 80131, Italy*

^{al}*INFN Torino, Torino 10125, Italy*

^{am}*Physics Department, Sapienza Università di Roma, Roma 00185, Italy*

^{an}*Physics Department, Università degli Studi di Salerno, Salerno 84084, Italy*

^{ao}*INFN Salerno, Salerno 84084, Italy*

^{ap}*Saint Petersburg Nuclear Physics Institute, Gatchina 188350, Russia*

^{aq}*Department of Physics, Engineering Physics and Astronomy, Queen's University, Kingston, ON K7L 3N6, Canada*

^{ar}*National Research Centre Kurchatov Institute, Moscow 123182, Russia*

^{as}*Physics Department, Lancaster University, Lancaster LA1 4YB, UK*

^{at}*APC, Université de Paris, CNRS, Astroparticule et Cosmologie, Paris F-75013, France*

^{au}*Museo Storico della Fisica e Centro Studi e Ricerche Enrico Fermi, Roma 00184, Italy*

^{av}*Institute for Particle Physics, ETH Zürich, Zürich 8093, Switzerland*

^{aw}*LPNHE, CNRS/IN2P3, Sorbonne Université, Université Paris Diderot, Paris 75252, France*

^{ax}*Williams College, Physics Department, Williamstown, MA 01267 USA*

^{ay}*Department of Physics and Astronomy, University of Hawai'i, Honolulu, HI 96822, USA*

^{az}*Fondazione Bruno Kessler, Povo 38123, Italy*

^{ba}*Trento Institute for Fundamental Physics and Applications, Povo 38123, Italy*

^{bb}*National Research Nuclear University MEPhI, Moscow 115409, Russia*

^{bc}*Joint Institute for Nuclear Research, Dubna 141980, Russia*

^{bd}*Institute of High Energy Physics, Beijing 100049, China*

^{be}*Engineering and Architecture Faculty, Università di Enna Kore, Enna 94100, Italy*

^{bf}*INFN Laboratori Nazionali del Sud, Catania 95123, Italy*

^{bg}*Department of Physics, University of Alberta, Edmonton, AB T6G 2R3, Canada*

^{bh}*School of Physics and Astronomy, University of Edinburgh, Edinburgh EH9 3FD, UK*

^{bi}*Fermi National Accelerator Laboratory, Batavia, IL 60510, USA*

^{bj}*Radiation Physics Laboratory, Belgorod National Research University, Belgorod 308007, Russia*

^{bk}*Pharmacy Department, Università degli Studi "Federico II" di Napoli, Napoli 80131, Italy*

^{bl}*School of Physics and Astronomy, University of Birmingham, Edgbaston, B15 2TT, Birmingham, UK*

^{bm}*INFN Roma Tre, Roma 00146, Italy*

^{bn}*Mathematics and Physics Department, Università degli Studi Roma Tre, Roma 00146, Italy*

^{bo}*Virginia Tech, Blacksburg, VA 24061, USA*

^{bp}*Fundación ARAID, Universidad de Zaragoza, Zaragoza 50009, Spain*

^{bq}*Physics Department, Temple University, Philadelphia, PA 19122, USA*

^{br}*Department of Physics, University of Liverpool, The Oliver Lodge Laboratory, Liverpool L69 7ZE, UK*

^{bs}*University of Warwick, Department of Physics, Coventry CV47AL, UK*

^{bt}*Budker Institute of Nuclear Physics, Novosibirsk 630090, Russia*

^{bu}*Novosibirsk State University, Novosibirsk 630090, Russia*

^{bv}*Amherst Center for Fundamental Interactions and Physics Department, University of Massachusetts, Amherst, MA 01003, USA*

^{bw}*Department of Physics and Astronomy, The University of Manchester, Manchester M13 9PL, UK*

^{bx}*Physics Department, Università degli Studi di Milano, Milano 20133, Italy*

^{by}*Department of Physics, University of Houston, Houston, TX 77204, USA*

^{bz}*Chemical, Materials, and Industrial Production Engineering Department, Università degli Studi "Federico II" di Napoli, Napoli 80126, Italy*

^{ca}*Department of Electronics and Communications, Politecnico di Torino, Torino 10129, Italy*

^{cb}*Physics and Astronomy Department, University of California, Los Angeles, CA 90095, USA*

^{cc}*University of Chinese Academy of Sciences, Beijing 100049, China*

^{cd}*Department of Physics and Astronomy, University of California, Riverside, CA 92507, USA*

^{ce}*Department of Physics and Engineering, Fort Lewis College, Durango, CO 81301, USA*

Abstract

The activation of materials due to exposure to cosmic rays may become an important background source for experiments investigating rare event phenomena. DarkSide-20k, currently under construction at the Laboratori Nazionali del Gran Sasso, is a direct detection experiment for galactic dark matter particles, using a two-phase liquid-argon Time Projection Chamber (TPC) filled with 49.7 tonnes (active mass) of Underground Argon (UAr) depleted in ^{39}Ar . Despite the outstanding capability of discriminating γ/β background in argon TPCs, this background must be considered because of induced dead time or accidental coincidences mimicking dark-matter signals and it is relevant for low-threshold electron-counting measurements. Here, the cosmogenic activity of relevant long-lived radioisotopes induced in the experiment has been estimated to set requirements and procedures during preparation of the experiment and to check that it is not dominant over primordial radioactivity; particular attention has been paid to the activation of the 120 t of UAr used in DarkSide-20k. Expected exposures above ground and production rates, either measured or calculated, have been considered in detail. From the simulated counting rates in the detector due to cosmogenic isotopes, it is concluded that activation in copper and stainless steel is not problematic. The activity of ^{39}Ar induced during extraction, purification and transport on surface is evaluated to be 2.8% of the activity measured in UAr by DarkSide-50 experiment, which used the same underground source, and thus considered acceptable. Other isotopes in the UAr such as ^{37}Ar and $^{3\text{H}}$ are shown not to be relevant due to short half-life and assumed purification methods.

Keywords: Cosmogenic activation, Argon, Dark matter, Rare events

¹ 1. Introduction

² Great efforts have been devoted worldwide to unravel the nature of dark
³ matter [1] which is expected to fill our galaxy. One strategy is to search

4 for Weakly Interacting Massive Particles (WIMPs) by direct detection via
 5 WIMP-nucleus elastic scattering using of different kinds of sensitive radiation
 6 detectors [2, 3]. Noble elements like xenon and argon are ideal targets because
 7 the material is easily purified and detectors can be scaled in mass for high
 8 sensitivity. [4–10].

9 The expected counting rate from the interaction of WIMPs is extremely
 10 low, requiring ultra-low background conditions. This is achieved by operating
 11 in deep underground locations, using active and passive shielding, carefully
 12 selecting radiopure materials, and developing background-rejection methods
 13 in analysis [11, 12]. In this context, long-lived radioactive isotopes induced
 14 in the materials of the experiment by the exposure to cosmic rays during fab-
 15 rication, transport and storage can be as relevant as residual contamination
 16 from primordial nuclides. In principle, cosmogenic activation can be kept
 17 under control by minimizing exposure on the surface and storing materials
 18 underground, avoiding flights, and even using shielding against the hadronic
 19 component of cosmic rays. It would be desirable to have reliable estimates
 20 of activation yields to assess the real danger of exposing materials to cosmic
 21 rays. Direct assay measurements of exposed materials, in very low back-
 22 ground conditions, and calculations of production rates and yields, following
 23 different approaches, have been made for several materials in the context of
 24 dark matter, neutrinoless 2β decay, and solar neutrino experiments [13, 14].
 25 Results have been calculated for detector media such as germanium [15–23],
 26 silicon [24], NaI [20, 25–28], tellurium and TeO_2 [29–31], xenon [32–34], ar-
 27 gon [20, 35, 36] and molybdate [37] as well as for copper [18, 32, 33, 38, 39],
 28 lead [40] or stainless steel [33, 38].

29 Liquid Argon (LAr) provides an outstanding Pulse Shape Discrimina-
 30 tion (PSD) power to separate electron recoils (ER) from nuclear recoil (NR)
 31 events, as shown by the single-phase LAr detector DEAP-3600 [7]. Dual-
 32 phase Time Projection Chambers (TPCs) have additional capabilities like
 33 excellent spatial resolution. The DarkSide-50 experiment at the Laboratori
 34 Nazionali del Gran Sasso (LNGS) in Italy followed this approach using Un-
 35 derground Argon (UAr) (depleted of ^{39}Ar by a factor 1400 ± 200 with respect
 36 to the Atmospheric Argon (AAr) activity of $\sim 1 \text{ Bq/kg}$) [8–10]. Despite these
 37 excellent background discrimination capabilities, acceptance losses (via ER
 38 + NR pile-up in the TPC or accidental coincidence between the Veto and
 39 TPC signals that mimic the neutron capture signature) can be produced by
 40 γ or β emitters in the set-up; therefore, these background sources must be
 41 carefully considered too. The goal of this work is, considering exposure on

42 the Earth's surface under realistic conditions, to quantify the yields of cosmogenic activation of detector materials and the effect on the expected counting
 43 rates of the DarkSide-20k detector; the results will be compared with those
 44 from other radioactive backgrounds like ^{39}Ar . This allows requirements and
 45 procedures during the preparation and commissioning of the experiment to
 46 be set. The study has been carried out for UAr as well as for copper, and
 47 stainless steel, since the use of large quantities of these materials is foreseen
 48 in different components, according to the design of DarkSide-20k. The paper
 49 is structured as follows: the DarkSide-20k project is presented in Sec. 2; the
 50 methodology applied to quantify cosmogenic activities is described in Sec. 3,
 51 showing the obtained results for different materials in Secs. 4 and 5; the
 52 counting rates expected from these activities are discussed in Sec. 6, before
 53 summarizing conclusions in Sec. 7.

55 2. The GADMC and the DarkSide-20k detector

56 The Global Argon Dark Matter Collaboration (GADMC) has been established to push the sensitivity for WIMP detection down through the neutrino
 57 fog [41, 42]. The first step will be the DarkSide-20k experiment at LNGS;
 58 the data taking is intended to start in 2026. The experiment is designed with
 59 a goal of an instrumental background <0.1 events over a 200 t·y exposure
 60 for a fiducial mass of 20 t. In parallel, a much smaller detector specifically
 61 optimized for the investigation of low-mass dark matter, DarkSide-LowMass,
 62 is being considered [43]. ARGO will be a multi-hundred tonne detector possibly
 63 operated at SNOLAB, having also excellent sensitivity to CNO neutrinos
 64 and galactic supernovae [44].

66 2.1. Underground Argon

67 One of the goals of GADMC is the procurement of large amounts of low-
 68 radioactivity UAr as detector target; three projects are in development to
 69 ensure this:

- 70 • Extraction of argon from an underground source (CO_2 wells) will be
 71 carried out at the Urania plant, in Cortez, CO (US). This is the same
 72 source used for the DarkSide-50 detector.
- 73 • UAr will be further chemically purified to detector-grade argon in the
 74 Aria facility, in Sardinia (Italy), to remove non-Argon isotopes. Aria
 75 will consist of a 350 m cryogenic distillation column, currently being

76 installed. Isotopic distillation with a short version of this column was
 77 demonstrated both with nitrogen [45] and argon isotopes [46]. Aria can
 78 also be operated in isotopic separation mode to achieve a 10-fold sup-
 79 pression of ^{39}Ar although at a much reduced throughput [46]; this fur-
 80 ther suppression beyond UAr level is not needed to achieve the physics
 81 goals of DarkSide-20k.

82 • Assessing the ultra-low ^{39}Ar content of the UAr is the the goal of the
 83 DArT detector [47] in construction at the Canfranc Underground Lab-
 84 oratory (LSC) in Spain.

85 There is a growing interest in the use of ultra-pure UAr outside GADMC,
 86 as it has potential broader applications for measuring coherent neutrino scat-
 87 tering in the COHERENT experiment [48], neutrinoless 2β decay in the
 88 LEGEND-1000 project [49], and future modules of the DUNE experiment
 89 [50]; the challenges for its production and characterization are carefully ad-
 90 dressed in Refs. [51, 52].

91 *2.2. DarkSide-20k*

92 In DarkSide-20k the core of the apparatus is a dual-phase TPC, serving
 93 both as active WIMP target, filled by low-radioactivity UAr [53]; a total
 94 of 99.2 t of UAr is required, 51.1 t inside the TPC and the rest in the
 95 neutron veto. It is planned to produce 120 t of UAr considering contingency.
 96 SiPMs in Photo-Detector Modules (PDMs) read the prompt scintillation in
 97 the liquid (S1) and delayed electroluminescence in the gas phase (S2). The
 98 TPC walls is made of a gadolinium-loaded acrylic vessel (Gd-PMMA); this
 99 material is highly efficient at moderating and then capturing neutrons, the
 100 capture resulting in the emission of several γ -rays that allow to tag neutron-
 101 induced background events. The detector is housed within a 12-ton vessel,
 102 made of stainless steel, immersed in a bath of 700 t of AAr acting as radiation
 103 shield and outer veto detector for cosmic background. All the materials used
 104 to build the whole detector system are carefully selected for low levels of
 105 radioactivity. Figure 1 shows cross views of the cryostat and of the inner
 106 detector. Table 1 lists materials, masses and considered cosmogenic isotopes
 107 for the main components in the design.

108 G4DS [54] is a Monte Carlo (MC) simulation framework developed for
 109 DarkSide background studies based on GEANT4, providing accurate simu-
 110 lation of light production, propagation, and detection for background and

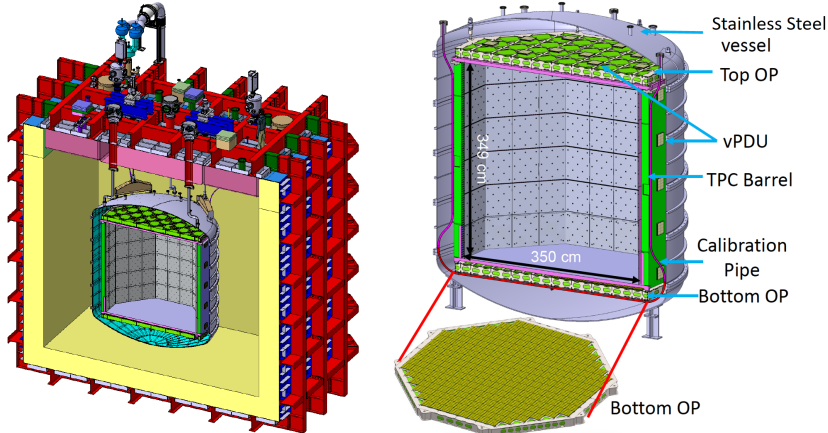


Figure 1: Cross sections of the cryostat (left) and of the vessel containing the inner veto and TPC (right) of the DarkSide-20k detector. OP stands for Optical Plane and vPDU for veto Photo Detection Unit.

Table 1: Detector components, materials and masses of the DarkSide-20k detector shown in Fig. 1. Cosmogenically-induced isotopes considered for each material in this work are also indicated; activation in Gd-loaded PMMA has not been analyzed as no hint was found in the radiopurity measurements by γ spectroscopy performed for acrylic and Gd_2O_3 samples.

Component	Material	Mass	Induced isotopes
Membrane cryostat	Stainless steel	224.6 t	See Table 2
Outer Veto: filling	AAr	700 t	^{37}Ar , ^{39}Ar , ^3H
Inner Veto: vessel	Stainless steel	12 t	See Table 2
TPC: barrel	Gd-loaded PMMA	11 t	-
TPC: grids, frame, brackets	Stainless steel	1055 kg	See Table 2
TPC: cables	Copper	117.8 kg	See Table 2
Inner Veto+TPC: filling	UAr	99.2 t	^{37}Ar , ^{39}Ar , ^3H
Electronic boards	Copper	47.3 kg	See Table 2

111 signal events; it has been extensively validated on DarkSide-50 data [54].
 112 For DarkSide-20k, γ emissions from the full set of detector components have
 113 been simulated to estimate the corresponding background rates in the TPC
 114 and in the Veto; activities measured in an extensive material screening cam-
 115 paign based on the combination of different radioassay techniques have been
 116 considered. Discrimination techniques based on energy and position of the
 117 interactions are implemented to compute the rate in the fiducial volume. As
 118 used in [44], preliminary estimates of γ background rates point to values
 119 around 50 Hz in the TPC and 100 Hz in the neutron Veto, with dominant
 120 contribution from PDMs. The β contribution of ^{39}Ar , considering the total
 121 active mass of UAr in the TPC (50 tonnes) and in the inner veto (32 tonnes)
 122 and the measured activity value in DarkSide-50, yields 36 Hz in the TPC
 123 and 26 Hz in the Veto. In this work, cosmogenically induced background
 124 shall be compared to these expected rates from radiogenic background from
 125 detector material.

126 3. Methodology

127 One of the most relevant processes in the production of radioactive iso-
 128 totes in materials is the spallation of nuclei by high energy nucleons; other
 129 reactions like fragmentation, induced fission or capture can be important for
 130 some nuclei too. On Earth's surface, as the proton to neutron ratio in cosmic
 131 rays decreases significantly at energies below the GeV scale because of the
 132 absorption of charged particles in the atmosphere, activation by neutrons is
 133 usually dominant. Cosmogenic production of radionuclides underground can
 134 often be considered negligible, as the flux of cosmic nucleons is suppressed
 135 by more than four orders of magnitude for depths of a few tens of meters
 136 water equivalent (m.w.e.) [11]. Radiogenic neutrons, with fluxes in deep un-
 137 derground facilities that are orders of magnitude lower than that of cosmic
 138 neutrons on surface, have energies around a few MeV, too low for spallation
 139 processes.

140 To quantify the effect of material cosmogenic activation in a particular
 141 experiment, the first step is to know the production rates, R , of the relevant
 142 isotopes induced in the material targets. Then, the produced activity, A , can
 143 be estimated according to the exposure history to cosmic rays; for instance,
 144 considering just a time of exposure t_{exp} followed by a cooling time (time spent
 145 underground once shielded from cosmic rays) t_{cool} , for an isotope with decay

¹⁴⁶ constant λ , the activity can be evaluated as:

$$A = R[1 - \exp(-\lambda t_{exp})] \exp(-\lambda t_{cool}). \quad (1)$$

¹⁴⁷ Finally, the counting rate generated in the detector by this activity can be
¹⁴⁸ computed using G4DS [54].

¹⁴⁹ Some direct measurements of production rates at sea level have been
¹⁵⁰ carried out for a few materials from the saturation activity, obtained by
¹⁵¹ sensitive screening of samples exposed in well-controlled conditions or by
¹⁵² irradiating samples in high flux particle beams. However, in many cases,
¹⁵³ production rates must be evaluated from the flux of cosmic rays, ϕ , and
¹⁵⁴ the isotope production cross-section, σ , with both dependent on the particle
¹⁵⁵ energy E :

$$R = N_t \int \sigma(E) \phi(E) dE, \quad (2)$$

¹⁵⁶ where N_t is the number of target nuclei. The spread for different calculations
¹⁵⁷ of production rates is usually important, even within a factor 2 (see for
¹⁵⁸ instance Tables 4 and 5). In this work, measured production rates have
¹⁵⁹ been used whenever available and dedicated calculations have been performed
¹⁶⁰ otherwise.

¹⁶¹ 3.1. Cosmic ray flux

¹⁶² An analytic expression for the cosmic neutron spectrum at sea level is
¹⁶³ presented by Gordon et al in Ref. [55], deduced by fitting data from a set
¹⁶⁴ of measurements for energies above 0.4 MeV; with this parameterization,
¹⁶⁵ the integral flux from 10 MeV to 10 GeV is $3.6 \times 10^{-3} \text{ cm}^{-2} \text{ s}^{-1}$ (for New York
¹⁶⁶ City). In Ref. [56], a similar parametrization is provided as well as correction
¹⁶⁷ factors, f , to the flux when considering exposure at different locations, as
¹⁶⁸ flux depends on the altitude and geomagnetic rigidity. For example, outside
¹⁶⁹ LNGS at an altitude of ~ 1000 m, a correction factor $f = 2.1$ [18] is used.
¹⁷⁰ Alternatively, the EXPACS (“EXcel-based Program for calculating Atmo-
¹⁷¹ spheric Cosmic-ray Spectrum”) program² could be used to calculate fluxes
¹⁷² of nucleons, muons, and other particles for different positions and times in the
¹⁷³ Earth’s atmosphere; in this way, possible temporal variations of the cosmic
¹⁷⁴ rays fluxes are taken into account. Although precise EXPACS calculations
¹⁷⁵ are being considered, results presented here are based on the parameteriza-
¹⁷⁶ tion from Ref. [55] and correction factor from Ref. [56].

²EXPACS: <https://phits.jaea.go.jp/expacs/>.

177 *3.2. Production cross sections*

178 Measurements at fixed energies and calculations using different compu-
179 tational codes must be both be taken into account in evaluating $\sigma(E)$. The
180 following have been used in this work:

- 181 • The Experimental Nuclear Reaction Data database (EXFOR, CSISRS
182 in US) [57], which provides nuclear reaction data and then measured
183 production cross sections ³.
- 184 • The Silberberg and Tsao equations presented in Refs. [58–60], which
185 are semiempirical formulae derived from proton-induced reactions for
186 energies >100 MeV and integrated in different codes: COSMO [61],
187 YIELDX [60] and ACTIVIA [62].
- 188 • The MC simulation of the interaction between projectiles and nuclei,
189 which allows also computation of production cross sections. Many dif-
190 ferent models and codes have been developed and validated considering
191 the relevant processes. Evaluated libraries of production cross sections
192 have been elaborated, covering different types of reactions or projec-
193 tiles and different energies, like TENDL (TALYS-based Evaluated Nu-
194 clear Data Library)⁴ [63] (based on the TALYS code, for protons and
195 neutrons with energies up to 200 MeV); JENDL (Japanese Evaluated
196 Nuclear Data Library) [64] High Energy File⁵ (based on the GNASH
197 code, for protons and neutrons from 20 MeV to 3 GeV) is an exten-
198 sion of the JENDL-4.0/HE library including results up to 200 MeV;
199 HEAD-2009 (High Energy Activation Data) [65] (for protons and neu-
200 trons with higher energies, from 150 MeV up to 1 GeV) uses a selection
201 of models and codes (CEM, CASCADE/INPE, MCNP, etc.).

202 **4. Cosmogenic yields in Copper and Steel**

203 The effect on DarkSide-20k of cosmogenic activity in the components
204 made of copper and stainless steel, known to become activated [13, 14], is
205 analyzed here.

³EXFOR: <http://www.nndc.bnl.gov/exfor/exfor.htm>, <http://www-nds.iaea.org/exfor/exfor.htm>.

⁴https://tendl.web.psi.ch/tendl_2019/tendl2019.html

⁵JENDL HE library, <https://wwwnndc.jaea.go.jp/ftpnd/jendl/jendl40he.html>;
<https://wwwnndc.jaea.go.jp/jendl/jendl.html>

206 *4.1. Production rates*

207 The production rates of the radionuclides typically induced in these ma-
 208 terials have been selected from measured and calculated results available in
 209 the literature [13, 14]. Estimates using mainly ACTIVIA, GEANT4, and
 210 TALYS codes have been made. Saturation activities have been measured
 211 with sensitive germanium detectors in samples of copper [32, 38, 39] and
 212 steel [38], exposed for long times to cosmic rays. In particular, in this work,
 213 the production rates from dedicated measurements, using 125 kg of copper
 214 provided by Norddeutsche Affinerie (now Aurubis) exposed for 270 days at
 215 Gran Sasso and Nironit stainless steel exposed for 314 days, have been con-
 216 sidered [38]; values are reproduced in Table 2. Among the different products
 217 identified in copper, ^{60}Co has the longest half-life and, unfortunately, there
 218 is a significant disagreement on the production rate estimates [13, 14]; the
 219 measured value in Ref. [38] is higher than most of the other estimates by a
 220 factor of up to a few times. No assessment of ^{60}Co production in stainless
 221 steel is made in Ref. [38], as the cosmogenically induced activity is shadowed
 222 by the intrinsic ^{60}Co at similar level naturally occurring in typical stainless
 223 steel material; for this reason, the rate derived from GEANT4 calculations
 224 [33] has been used. Following the half-lives of the different cosmogenic iso-
 225 topes identified in copper and steel (also shown in Table 2), ^{54}Mn , ^{57}Co and
 226 ^{60}Co are in principle the most relevant products.

227 *4.2. Activity*

228 To assess the possible effect of the cosmogenic isotopes in these mate-
 229 rials for DarkSide-20k, activity A has been evaluated considering the se-
 230 lected production rates at sea level, $t_{cool} = 0$ and extreme cases of exposure:
 231 $t_{exp} = 1$ month, $t_{exp} = 1$ year and $t_{exp} = 10$ years. It is worth noting that as
 232 measured production rates have been taken into account, the deduced acti-
 233 vation corresponds to all cosmic ray particles. The final expected activity is
 234 obtained from the specific activities derived from the production rates (per
 235 mass unit) using Eq. 1 and the mass of all the components used in the
 236 experimental set-up, which according to the present design of DarkSide-20k
 237 are 165.1 kg of copper (mainly from cables and PDMs electronic compo-
 238 nents) and 226 tons of stainless steel (mainly from cryostat components)
 239 plus 12 tonnes from the inner detector.

240 Table 2 summarizes the total induced activity in copper and stainless
 241 steel, respectively, for the relevant isotopes evaluated at the end of the differ-
 242 ent exposure times; contribution from each individual component is propor-

tional to its mass (see Table 1). Following the decay mode of these nuclei, γ emissions of the order of 1 MeV will be generated around the active volume by this cosmogenic activation. In the case of copper, even assuming 10 years of exposure, the total activity is at the level of 0.5 Bq. The induced activities are then compared with available measurements from radioassays. For the copper from the Luvata company which is being considered in DarkSide-20k, upper limits of 0.30 mBq/kg of ^{60}Co and 0.35 mBq/kg of ^{54}Mn are obtained using a HPGe detector (named GeOroel) in the Canfranc Underground Laboratory. Exposure to cosmic rays of this copper material for a few years can be tolerated since it would contribute a fraction of the upper limit on ^{60}Co contamination. For all stainless steel components, some cosmogenic activities can be at the level of a few hundreds of Bq, even for just 1 year of exposure; ^{54}Mn is identified as a potential relevant contributor to the background. Comparing with available measurements from screening, the derived cosmogenic activity of ^{60}Co is much lower than for instance the one measured for a sample of stainless steel for the DarkSide-20k cryostat, using the same HPGe detector in the Canfranc Underground Laboratory, finding (10.8 ± 0.9) mBq/kg of ^{60}Co . A more stringent requirement of ~ 1 year of exposure would come by requiring the ^{54}Mn induced activity being less than the measured one in radio-assay of (1.4 ± 0.3) mBq/kg.

Table 2: Estimates of induced activity in copper and stainless steel components of DarkSide-20k at the end of the exposure to cosmic rays. For each product, the half-life [66], main γ emissions and corresponding probabilities are indicated together with the production rates R at sea level considered (from measurements in Ref. [38] except for ^{60}Co in stainless steel, taken from Ref. [33]) and the total activity A for the three exposure times considered (1 month, 1 year and 10 years).

	^{7}Be	^{46}Sc	^{54}Mn	^{59}Fe	^{56}Co	^{57}Co	^{58}Co	^{60}Co
$T_{1/2}$ (d)	53.22	83.79	312.19	44.49	77.24	271.82	70.85	1923.95
γ emissions (keV)	477.6	889.3, 1120.5	834.8	1099.3, 1291.6	846.8, 1238.3	122.1	810.8	1173.2, 1332.5
probability (%)	10.5	99.98, 99.98	99.98	56.5, 43.2	100, 67.6	85.6	99	99.97, 99.99
Copper								
R (atoms/kg/day)	2.18 \pm 0.74	8.85 \pm 0.86	18.7 \pm 4.9	9.5 \pm 1.2	74 \pm 17	67.9 \pm 3.7	86.4 \pm 7.8	
A (1 m) (mBq)	0.92 \pm 0.31	1.09 \pm 0.11	13.3 \pm 3.5	4.28 \pm 0.54	10.4 \pm 2.4	33.0 \pm 1.8	1.77 \pm 0.16	
A (1 y) (mBq)	4.0 \pm 1.3	9.39 \pm 0.91	35.6 \pm 9.3	17.5 \pm 2.2	86 \pm 20	126.1 \pm 6.9	20.3 \pm 1.8	
A (10 y) (mBq)	4.2 \pm 1.4	16.9 \pm 1.6	35.7 \pm 9.4	18.2 \pm 2.3	141 \pm 32	129.8 \pm 7.1	121 \pm 11	
Stainless Steel								
R (atoms/kg/day)	389 \pm 60	19.0 \pm 3.5	233 \pm 26	20.7 \pm 3.5	51.8 \pm 7.8	6.27		
A (1 m) (Bq)	346 \pm 53	11.5 \pm 2.1	41.3 \pm 4.6	13.4 \pm 2.3	36.2 \pm 5.5	0.19		
A (1 y) (Bq)	1061 \pm 164	49.7 \pm 9.2	356 \pm 40	54.8 \pm 9.3	138 \pm 21	2.1		
A (10 y) (Bq)	1070 \pm 165	52.3 \pm 9.6	641 \pm 71	56.9 \pm 9.6	142 \pm 21	13		

263 **5. Cosmogenic yields in Argon**

264 Argon in the atmosphere contains stable ^{40}Ar at 99.6%; cosmogenically
 265 produced radioactive isotopes, mainly ^{39}Ar but also ^{37}Ar or ^{42}Ar , can be a
 266 significant background if argon obtained from air is used. The concentra-
 267 tion of these three isotopes is much reduced in UAr, but the production of
 268 cosmogenic radionuclides after extraction must be taken into consideration.

269 *5.1. Relevant isotopes*

270 ^{39}Ar is a β^- emitter with a transition energy of 565 keV and half-life of
 271 269 y [67]; it is mainly produced by the $^{40}\text{Ar}(n,2n)^{39}\text{Ar}$ reaction by cosmic
 272 neutrons [35]. The typical activity of ^{39}Ar in AAr is at the level of $\sim 1 \text{ Bq/kg}$,
 273 as measured by WARP [68], ArDM [69] and DEAP [70]. In UAr, after a first
 274 study on argon from deep underground sources [71], the measured activity
 275 of ^{39}Ar in the DarkSide-50 detector was $(0.73 \pm 0.11) \text{ mBq/kg}$ following a
 276 campaign of extracting and purifying argon from deep CO₂ wells in Colorado,
 277 US; as mentioned in Sec. 1, this means a reduction of a factor $(1.4 \pm 0.2) \times 10^3$
 278 relative to the AAr [8].

279 The presence of cosmogenically produced ^{37}Ar was also detected at the
 280 beginning of the run of the DarkSide-50 detector with UAr [8]. It decays
 281 100% by electron capture to the ground state of the daughter nuclei with a
 282 half-life of 35.02 days [66]; then, the binding energy of electrons from K-shell
 283 (2.8 keV, at 90.21%) and L-shell (0.20-0.27 keV, at 8.72%) can be measured
 284 as a distinctive signature. The main production channel is the $^{40}\text{Ar}(n,4n)^{37}\text{Ar}$
 285 reaction [35]. Underground production in UAr by thermal and epithermal
 286 neutron capture is negligible, as for ^{39}Ar , considering rates as in Ref. [35]
 287 and neutron fluxes at LNGS.

288 ^{42}Ar is a pure β^- emitter with a 32.9 y half-life and transition energy
 289 of 599 keV, generating ^{42}K , also a β^- emitter with half-life of 12.36 h and
 290 transition energy of 3525 keV [67]; this isotope can affect neutrinoless 2β
 291 experiments using liquid argon as cooling bath and shielding, as shown
 292 by the GERDA experiment [72] and its specific activity has been studied
 293 by ICARUS [73], DBA ($92^{+22}_{-46} \mu\text{Bq/kg}$ [74]) and DEAP ($40.4 \pm 5.9 \mu\text{Bq/kg}$
 294 [70]). The production rate of ^{42}Ar in UAr at sea level has been evaluated by
 295 GEANT4 simulation as 5.8×10^{-3} atoms/kg/day in Ref. [36]; this rate would
 296 give from Eq. 1 a saturation activity of $0.07 \mu\text{Bq/kg}$, about three orders of
 297 magnitude lower than measured values in AAr. Taking all this into account,

298 the effect of ^{42}Ar in DarkSide-20k will not be considered here although a spe-
 299 cific study to quantify radiogenic and cosmogenic production in the Earth's
 300 crust is underway⁶.

301 ^3H is a pure β^- emitter with transition energy of 18.6 keV and a long
 302 half-life of 12.3 y [66]. The quantification of its cosmogenic production is
 303 not easy by calculations (^3H can be generated by different reaction chan-
 304 nels) nor experimentally (the β emissions are hard to disentangle from other
 305 background contributions). Estimates of the ^3H production rate in several
 306 dark matter targets were attempted in Ref. [20]; the rate has been measured
 307 for germanium from EDELWEISS [19] and CDMSlite [21] data and for sil-
 308 icon and NaI(Tl) from neutron irradiation [24, 28]. The possible presence
 309 of ^3H has been observed also in NaI(Tl) crystals by the ANAIS [25, 75] and
 310 COSINE experiments [27, 76]. In principle, purification systems for LAr
 311 may remove all non-argon radionuclides and ^3H should not be a problem for
 312 DarkSide. This was also assumed for liquid xenon, but ^3H was considered
 313 as a possible explanation for the excess of electronic recoil events observed
 314 in the XENON1T experiment below 7 keV [77, 78], which was not observed
 315 in XENONnT [5]. Activated ^3H is separated from argon with SAES Getters
 316 [79] and will be removed *in situ* while the UAr recirculates.

317 Other radioisotopes with half-lives longer than 10 days like ^7Be , ^{10}Be ,
 318 ^{14}C , ^{22}Na , ^{26}Al , ^{32}P , ^{33}P , ^{32}Si , ^{35}S , ^{36}Cl , ^{40}K and ^{41}Ca are also produced
 319 in argon, as shown using the COSMO code. The production rates of these
 320 isotopes at sea level from fast neutrons, high energy muons and protons have
 321 been evaluated by GEANT4 simulation in Ref. [36]. Assuming an efficient
 322 purification of non-noble isotopes, they will not be considered in this study.

323 5.2. Production rates

324 The production rates of ^{37}Ar and ^{39}Ar from cosmic neutrons at sea level
 325 were measured for the first time through controlled irradiation at Los Alamos
 326 Neutron Science Center (LANSCE) with a neutron beam resembling the cos-
 327 mic neutron spectrum and later direct counting with sensitive proportional
 328 counters at Pacific Northwest National Laboratory (PNNL) [35]. In addition,
 329 the study of other production mechanisms due to muon capture, cosmic pro-
 330 tons and high energy γ rays at the Earth's surface was made using available
 331 cross sections to compute total production rates at sea level. The production

⁶<https://indico.sanfordlab.org/event/29/contributions/487/>

Table 3: Calculation of the correction factor f to be applied to the cosmic neutron flux at sea level (in New York) for the location of the Urania facilities in Colorado. The relative intensities I are derived from Eq. 3. The final factor for Urania is the average between the deduced ones from Denver and Leadville data.

Location	H (m)	A (g/cm^2)	f from Ref. [56]	Relative I to Urania	Deduced f for Urania
Denver	1609	852.3	4.11	0.659	6.24
Leadville	3109	705.2	12.86	1.942	6.62
Urania	2164	795.5			6.43

332 rates obtained in Ref. [35] for UAr are reproduced in Table 6 as they will
 333 be used to evaluate the induced activity in DarkSide-20k. The production
 334 rates of both ^{37}Ar and ^{39}Ar at sea level were also evaluated by GEANT4
 335 simulation in Ref. [36].

336 The UAr to be used in DarkSide-20k is extracted in Colorado, at a quite
 337 high altitude, so the corresponding correction factors f to the cosmic ray flux
 338 at sea level must be taken into consideration. In Ref. [56], high values of f
 339 are reported for neutrons at Colorado locations: 4.11 and 12.86 for Denver
 340 (at 1609 m) and Leadville (at 3109 m), respectively. These correction factors
 341 f have been adjusted to the altitude at the Urania facilities (at 2164 m),
 342 assuming that the ratio of f for different altitudes is the same as the ratio of
 343 cosmic flux intensities. As described in Ref. [56], the intensities I_1 and I_2 at
 344 two different altitudes A_1 and A_2 (converted to g/cm^2) are related as:

$$I_2 = I_1 \exp[(A_1 - A_2)/L], \quad (3)$$

345 being L the absorption length for the cosmic ray particles. Calculations for
 346 the cosmic neutron flux correction factor are summarized in Table 3, using
 347 $L = 136 \text{ g}/\text{cm}^2$; the final result for Urania is the average between those from
 348 Denver and Leadville data, $f = 6.43$. For cosmic protons and muons, the
 349 correction factors have been obtained just from Eq. 3 considering the corre-
 350 sponding absorption lengths ($L = 110 \text{ g}/\text{cm}^2$ for protons and $L = 261 \text{ g}/\text{cm}^2$
 351 for muons [56]); the results are $f = 8.67$ for protons and $f = 2.48$ for muons.

352 Following Eq. 2, a calculation of the production rates of relevant iso-
 353 topes in argon (assuming 100% ^{40}Ar) by cosmic neutrons from Ref. [55] has
 354 been made considering a selection of excitation functions from libraries and
 355 YIELDX calculations. Figure 2 shows our compilation of production cross
 356 sections of ^3H , ^{37}Ar and ^{39}Ar by nucleons. For ^{39}Ar , although no experimen-
 357 tal data at EXFOR was found for the total production cross section, there are

358 results for partial ($n,2n\gamma$) reactions in natural argon at 1-30 MeV taken from
 359 Ref. [80]. For 3H , an irradiation experiment with neutrons having an energy
 360 spectrum peaked at 22.5 MeV measured the corresponding production cross
 361 section [81].

362 A mismatch between cross section data from different libraries is observed.
 363 Several descriptions of the cross sections, even from different libraries below
 364 and above a particular energy cut, have been considered to estimate the
 365 corresponding uncertainty; the obtained maximum and minimum rates define
 366 an interval, whose central value and half width have been considered as the
 367 final result and its uncertainty for the evaluation of the production rates.
 368 Table 4 presents the obtained results for ^{37}Ar and ^{39}Ar , together with the
 369 measured production rate for fast neutrons and different calculations from
 370 Refs. [35, 36]. The production rate of ^{39}Ar derived here is fully compatible
 371 with the measured value (and with several of the calculations in Ref. [35]).
 372 The production rate of ^{37}Ar is a factor 2 higher than the measured one,
 373 but lower than the GEANT4 estimate in Ref. [36]. For calculating the final
 374 activity yields of ^{37}Ar and ^{39}Ar , the values of the total production rates
 375 obtained in Ref. [35] will be used; but this comparison can be useful to
 376 assess the reliability of the production rates of isotopes estimated only from
 377 calculations, like 3H in argon.

378 The production rate of 3H in argon was calculated, as for other targets,
 379 using different codes like TALYS [16] and GEANT4 and ACTIVIA [33]. It
 380 was also computed in Ref. [20] using a similar approach as used in this
 381 work from a selection of excitation functions considering the TENDL and
 382 HEAD2009 libraries. The results ranged from 115.1 to 177.2 atoms/kg/day
 383 and the approach was cross-checked against experimental data for NaI and
 384 germanium, reproducing properly measured production rates [19, 21, 28].
 385 We add to the analysis new data included in the JENDL-HE library which
 386 gives a production rate of 221.6 atoms/kg/day. We combine the results in
 387 Ref. [20] with this latter one to estimate a central value and uncertainty
 388 for the production of 3H as (168 ± 53) atoms/kg/day. It must be noted that
 389 this value gives only production by neutrons; assuming equal flux and cross
 390 sections of protons and neutrons above 1 GeV, it is estimated that protons
 391 would increase the rate by 10% at most [20] and is thus neglected in the
 392 following. Table 5 compares the production rate estimated in this work with
 393 all the available ones for 3H production in argon taken from the literature
 394 following different approaches; an important dispersion of values is found.

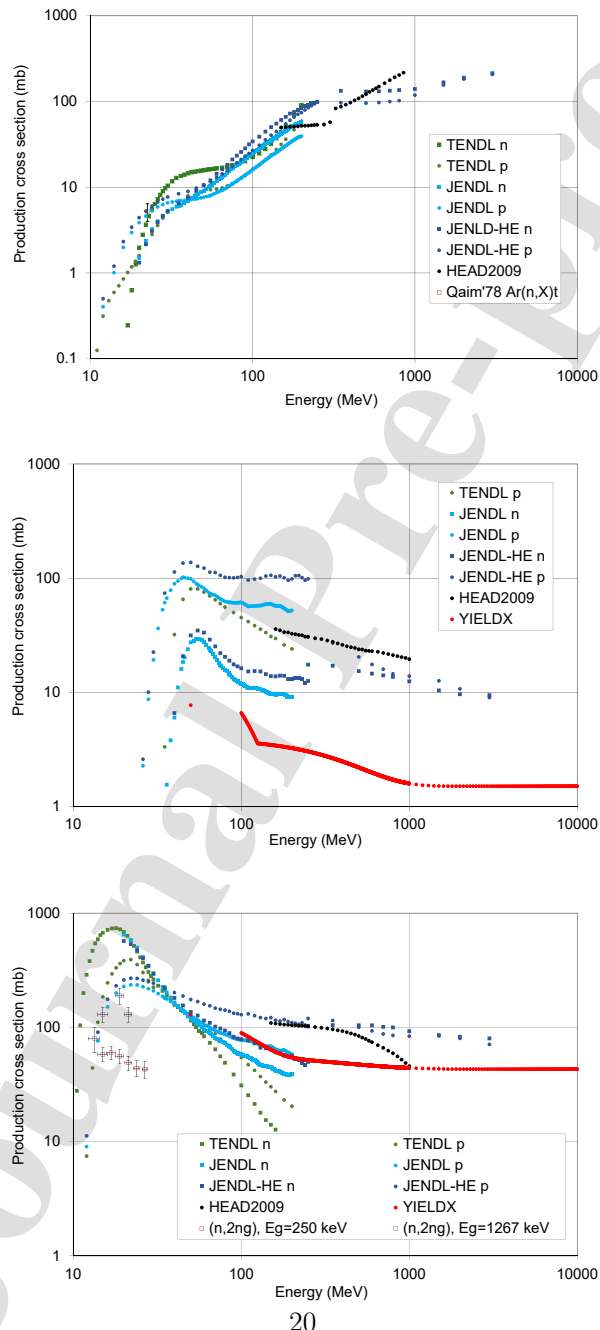


Figure 2: Production cross sections of ^3H (top), ^{37}Ar (middle) and ^{39}Ar (bottom) in ^{40}Ar by nucleons vs energy taken from different sources.

Table 4: Calculations of the production rates R of ^{37}Ar and ^{39}Ar in Ar at sea level from this work considering different descriptions of the excitation functions below (LE) and above (HE) a cut energy value; the final estimated rates are given by the ranges defined between the maximum and minimum obtained rates (see text). Different calculations from the literature (considering the same cosmic neutron spectrum from Ref. [55]) and the measured value for fast neutrons from Ref. [35] are also shown for comparison.

	^{37}Ar			^{39}Ar		
	Cut (MeV)	R (atoms/kg/day)	This work LE+HE	Cut (MeV)	R (atoms/kg/day)	
This work: LE+HE						
TENDL(p)+HEAD2009	150	153.6	TENDL+HEAD2009	150	726.4	
TENDL(p)+YIELDX	100	93.5	TENDL+YIELDX	100	697.1	
TENDL(p)+YIELDX	200	122.7	TENDL+YIELDX	200	646.0	
JENDL-HE(n)	30	63.9	TENDL+JENDL-HE(n)	20	804.3	
Estimated rate in this work		109±45	Estimated rate in this work		725±79	
Not used for estimation:						
Measurement [35]		51.0±7.4			759±128	
ACTIVIA [35]		17.9±2.2			200±25	
MENDL-2P [35]		155±19			188±24	
TALYS [35]		76.8±9.6			753±94	
INCL++ (ABLA07) [35]		79.3±9.9			832±104	
GEANT4 [36]		176			726±91	
					858	

Table 5: Production rate R of ${}^3\text{H}$ in Ar at sea level from this work and from different calculations from the literature.

	R (atoms/kg/day)
TENDL	115.1
HEAD2009	177.2
JENDL-HE	221.6
Estimated rate in this work	168 ± 53
Not used for estimation:	
TALYS [16]	44.4
GEANT4 [33]	84.9
ACTIVIA [33]	82.9

395 5.3. Activity

396 The possible activity yields of relevant cosmogenic isotopes in Ar have
 397 been analyzed for the DarkSide-20k detector considering Ar extraction, stor-
 398 age and transportation and taking into account different cosmic ray compo-
 399 nents. For ${}^{37}\text{Ar}$ and ${}^{39}\text{Ar}$, the production rates at sea level precisely deter-
 400 mined with the LANSCE neutron beam and the estimates for muons, protons
 401 and cosmic γ rays [35] have been considered, while for ${}^3\text{H}$ the production rate
 402 estimated in this work has been assumed.

403 The UAr extracted at the Urania plant will be shipped firstly to the Aria
 404 facility for purification and then to LNGS for storage and final operation.
 405 The current baseline design is to ship the UAr in high-pressure gas cylinders
 406 that are organized into skids capable of containing ~ 2 t of UAr each. The
 407 following steps are foreseen:

- 408 1. Storage of UAr at Urania: three skids will be filled before starting
 409 transportation. Considering the time required to fill one, exposures of
 410 8, 16 and 24 days have been assumed for each skid. At the Urania
 411 site, the UAr will always be on surface while being processed and once
 412 in the skids. The correction factors to the sea level fluxes of cosmic
 413 neutrons, protons and muons evaluated for Urania location in Colorado
 414 (see Sec. 5.2) have been included in this step.
- 415 2. Trip from Urania to a shipping port: a container with the three skids
 416 will transport the UAr from Urania to Houston, TX (USA), by road.
 417 An exposure of 7 days has been considered. To take into account the
 418 different altitude during the trip, the average between the maximal

419 (from Urania altitude) and minimal (at sea level) expected activity has
 420 been calculated.

421 3. Trip overseas to Europe: 60 days of exposure at sea level have been
 422 conservatively assumed for the trip by boat from Houston to Cagliari.
 423 An additional exposure of 7 days is foreseen for custom clearing and
 424 the trip from Cagliari to the Aria location.
 425 In total, 16 months are required for completing the extraction and
 426 transportation of all the necessary UAr from Urania to Italy.

427 4. Processing and storage of UAr at Aria: once in Sardinia, the skids will
 428 be stored near Aria and the UAr will be accumulated for processing.
 429 At a purification rate of 1 ton per day, an expected exposure of 60 days
 430 to process two batches of 60 t each has been considered. Underground
 431 storage at a depth of at least some tens of m.w.e. would be ideal and
 432 it is assumed here but, if not possible, an almost linear increase of
 433 2.6 μ Bq/kg in the activity of ^{39}Ar is estimated per month of additional
 434 exposure at sea level.

435 5. Trip from Aria to LNGS: 10 days of exposure at sea level have been
 436 considered for this trip by sea. It is expected to ship 12 t at a time
 437 using six skids.

438 6. Storage at LNGS: skids will be stored underground as they arrive.

439 Under these assumptions, the total time from the beginning of production
 440 at Urania to the end of processing at Aria is 614 days.

441 Taking into account this exposure history, the induced activity by each
 442 cosmic ray component has been computed for each exposure step (at Urania,
 443 trip in US, overseas, at Aria and trip in Italy) from Eq. 1. Tables 6 and
 444 7 show separately each contribution for ^{39}Ar and ^{37}Ar and for ^3H , respec-
 445 tively. Contributions from different cosmic ray components are assumed to
 446 be independent to derive uncertainties in total activity. The decrease of the
 447 activities induced at each step during the rest of the whole process is neg-
 448 ligible for ^{39}Ar and small for ^3H , due to their long half-lives, but extremely
 449 relevant for ^{37}Ar ; it is accounted for in the final activities reported in Tables
 450 6 and 7.

451 For both ^{39}Ar and ^{37}Ar , cosmogenic neutrons are responsible of most
 452 of the induced activity. Under the assumed conditions, the relative contribu-
 453 tions to the final ^{39}Ar activity of each exposure step are the following:
 454 Urania, 34.4%; US trip, 9.0%; overseas trip, 27.7%; at Aria, 24.8%; and Italy
 455 trip, 4.1%. The exposure at Urania gives the largest contribution, followed

456 by that of the overseas trip and at Aria. For ^{37}Ar , having a much shorter
 457 half-life, the last exposure during the Italy trip is dominant, producing 55%
 458 of the final activity. Concerning ^3H , the final activity in Table 7 would ap-
 459 ply if no purification procedures were considered; however, if a 100% efficient
 460 removal of ^3H was achieved in Aria, only the activity in the last step for expo-
 461 sure in Italy would be produced. Table 8 summarizes the expected activities
 462 once all the UAr is at LNGS. From values in Table 6, the final estimated
 463 activity of ^{39}Ar is $(20.7 \pm 2.8) \mu\text{Bq/kg}$; this equals 2.8% of measured activity
 464 in DarkSide-50. For ^{37}Ar , the effect of cooling is very important and the
 465 expected activity when all the UAr is at LNGS is $(103 \pm 14) \mu\text{Bq/kg}$. From
 466 values in Table 7 for ^3H , an activity of $(2.97 \pm 0.94) \mu\text{Bq/kg}$ is expected at
 467 that time considering only activation after ideal purification in Aria; with no
 468 purification, it would be around 25 times higher.

469 Uncertainties quoted for activities in Tables 6 and 7 come from those of
 470 production rates, reproduced in the same tables. Concerning the correction
 471 factors of sea level cosmic ray fluxes for exposure at Urania, it has been
 472 checked that considering a description different to that applied in Sec. 5.2
 473 produces very similar results; correction factors computed from EXPACS
 474 spectra in the energy range relevant for activation (1 MeV to 10 GeV) are
 475 $f = 6.09$ for neutrons, $f = 7.60$ for protons and $f = 1.61$ for muons, giving a
 476 small decrease in the final activities: 1.0% for ^{39}Ar , no change for ^{37}Ar and
 477 1.5% for ^3H with no purification. On the other hand, unexpected events can
 478 produce relevant deviations from the baseline exposure conditions and their
 479 effect on the activation yields has been assessed. Doubling the exposure
 480 at Urania would increase the final ^{39}Ar activity from $(20.7 \pm 2.8) \mu\text{Bq/kg}$
 481 to $(27.7 \pm 3.9) \mu\text{Bq/kg}$, which would be 3.8% of the DarkSide-50 activity.
 482 Exposure at Aria has been evaluated for the moment considering just the
 483 processing time, but activation produced in the periods before and after the
 484 processing should be added if storage is made above ground; to produce an
 485 additional 10% of the measured activity in DarkSide-50 (which was deter-
 486 mined with an uncertainty of 14%), 28 months of additional exposure would
 487 be required, which is well above the period of 16 months needed for the ex-
 488 traction of the whole amount of UAr needed. It can be concluded that there
 489 is enough contingency in the plan for production, storage and shipping of
 490 the UAr so that cosmogenic ^{39}Ar activity does not endanger DarkSide-20k
 491 sensitivity.

492 6. Expected counting rates in DarkSide-20k

493 The rates from the estimated cosmogenic activity of products in UAr,
494 under the assumed exposure conditions, are also shown in Table 8. Induced
495 ^{39}Ar due to the whole exposure from Urania to LNGS would add a rate of
496 (1.03 ± 0.14) Hz for the TPC. The contribution of ^{37}Ar (being (5.15 ± 0.68) Hz
497 if data taking started just immediately after the arrival of all the UAr at
498 LNGS) will decay very quickly. Comparing these numbers with the total
499 β and γ rates presented in Sec. 2.2, it can be concluded that cosmogenic
500 activity does not produce a problematic increase of the TPC and Veto rates.

501 7. Conclusions

502 For DarkSide-20k, material cosmogenic activation is a source of β/γ back-
503 ground and it has been quantified for LAr and other materials used in large
504 amounts from realistic exposure conditions in order to assess the contribu-
505 tion to the counting rates and decide if additional exposure restrictions are
506 necessary. The main results are summarized in Table 8.

Table 6: Calculation of the expected induced activity in $\text{kg}^{-1} \text{d}^{-1}$ of ^{39}Ar and ^{37}Ar in the UAr of the DarkSide-20k detector, for the assumed production rates R and exposure times (see text). Different columns and rows show separate contributions by cosmic ray components and exposure steps, respectively; relative contributions of each component to the total activity are also quoted. Row labelled as "Final" presents the sum of final activities from all exposure steps including properly their decays.

^{39}Ar	Neutrons	Muons	Protons	γ rays	Total
R (atoms/kg/day) [35]	759 ± 128	172 ± 26	3.6 ± 2.2	112.8 ± 20.9	
Urania	0.551 ± 0.093	0.0483 ± 0.0073	0.0035 ± 0.0022	0.0127 ± 0.0024	0.616 ± 0.093
US	0.139 ± 0.024	0.0148 ± 0.0022	0.0009 ± 0.0005	0.0056 ± 0.0010	0.161 ± 0.024
Overseas	0.359 ± 0.061	0.081 ± 0.012	0.0017 ± 0.0010	0.053 ± 0.010	0.495 ± 0.063
Aria	0.321 ± 0.054	0.073 ± 0.011	0.0015 ± 0.0009	0.048 ± 0.0088	0.444 ± 0.056
Italy	0.0536 ± 0.0090	0.0121 ± 0.0018	0.0003 ± 0.0002	0.0080 ± 0.0015	0.0739 ± 0.0093
Final (%)	1.42 ± 0.24 79.6	0.229 ± 0.035 12.8	0.0078 ± 0.0048 0.4	0.127 ± 0.024 7.1	1.79 ± 0.24

^{37}Ar	Neutrons	Thermal neutrons	Protons	γ rays	Total
R (atoms/kg/day) [35]	51 ± 7.4	0.9 ± 0.3	1.3 ± 0.4	3.5 ± 0.7	
Urania	87 ± 13	2.99 ± 0.92	0.93 ± 0.19	0.239 ± 0.080	91 ± 13
US	24.5 ± 3.6	0.81 ± 0.25	0.453 ± 0.091	0.116 ± 0.039	25.9 ± 3.6
Overseas	37.5 ± 5.4	0.95 ± 0.29	2.57 ± 0.51	0.66 ± 0.22	41.7 ± 5.5
Aria	35.5 ± 5.1	0.90 ± 0.28	2.43 ± 0.49	0.63 ± 0.21	39.4 ± 5.2
Italy	9.2 ± 1.3	0.234 ± 0.072	0.63 ± 0.13	0.162 ± 0.054	10.2 ± 1.3
Final (%)	8.0 ± 1.2 90.3	0.209 ± 0.064 2.3	0.52 ± 0.10 5.9	0.135 ± 0.045 1.5	8.9 ± 1.2

Table 7: Calculation of the expected induced activity in $\text{kg}^{-1} \text{d}^{-1}$ of ${}^3\text{H}$ by cosmic neutrons in the UAr of the DarkSide-20k detector, for the production rate R estimated in this work and the assumed exposure times (see text), considering no purification procedure. Different rows show separate contributions by exposure steps. Row labelled as “Final” presents the sum of final activities from all exposure steps including properly their decays.

${}^3\text{H}$	
R (atoms/kg/day)	168 ± 53
Urania	2.66 ± 0.84
US	0.67 ± 0.21
Overseas	1.73 ± 0.54
Aria	1.55 ± 0.49
Italy	0.259 ± 0.082
Final	6.5 ± 2.1

Table 8: Summary table of estimated activation in DarkSide-20k including isotope, material, calculation details, overall activity and counting rates in TPC and inner veto. The most relevant channel for each isotope are shown in the third column (although other ones are included). All reported activity and rate values correspond to the moment when the materials are brought underground. For ${}^3\text{H}$, row (1) and (2) assume no purification and ideal purification at Aria, respectively.

Isotope	Material	Most relevant channel	Calculation	Activity ($\mu\text{Bq}/\text{kg}$)	TPC rate (Hz)	Veto rate (Hz)
${}^{39}\text{Ar}$	UAr	${}^{40}\text{Ar}(\text{n},2\text{n}){}^{39}\text{Ar}$	Production rates from [35]	20.7 \pm 2.8	1.03 \pm 0.14	0.662 \pm 0.090
	UAr	${}^{40}\text{Ar}(\text{n},4\text{n}){}^{37}\text{Ar}$	Production rates from [35]	103 \pm 14	5.15 \pm 0.68	3.30 \pm 0.43
${}^{37}\text{Ar}$	UAr	${}^{40}\text{Ar}(\text{n},*){}^{37}\text{Ar}$	$\sigma(E)$ in Fig. 2+Gordon spectrum	76 \pm 24	3.8 \pm 1.2	2.42 \pm 0.76
	UAr	${}^{40}\text{Ar}(\text{n},*){}^{37}\text{Ar}$	$\sigma(E)$ in Fig. 2+Gordon spectrum	2.97 \pm 0.94	0.148 \pm 0.047	0.095 \pm 0.030
${}^3\text{H}$ (1)	UAr	${}^{40}\text{Ar}(\text{n},*){}^3\text{H}$	$\sigma(E)$ in Fig. 2+Gordon spectrum	76 \pm 24	3.8 \pm 1.2	2.42 \pm 0.76
	UAr	${}^{40}\text{Ar}(\text{n},*){}^3\text{H}$				
${}^3\text{H}$ (2)	UAr	${}^{40}\text{Ar}(\text{n},*){}^3\text{H}$	$\sigma(E)$ in Fig. 2+Gordon spectrum	2.97 \pm 0.94	0.148 \pm 0.047	0.095 \pm 0.030
	UAr	${}^{40}\text{Ar}(\text{n},*){}^3\text{H}$				

507 For copper and stainless steel components, activation yields of isotopes
 508 with relevant half-lives (like ^{54}Mn , ^{57}Co and ^{60}Co) have been computed from
 509 the measured production rates at sea level at Ref. [38]. In copper, even
 510 for 10 y of exposure to cosmic rays, estimated activities are below 0.5 Bq.
 511 In stainless steel, hundreds of Bq are expected for some isotopes for just
 512 1 y exposure; the contribution to the counting rate of ER-like events in the
 513 TPC from ^{54}Mn activity induced in steel components has been found to be
 514 negligible in comparison to the estimated total rate from β/γ backgrounds.
 515 This avoids restricting the surface residency time.

516 A total of 120 t of UAr depleted in ^{39}Ar must be extracted and processed
 517 for filling the TPC and inner veto of DarkSide-20k. The possible induced ac-
 518 tivity on surface, from the extraction at Urania to the storage at LNGS, has
 519 been analyzed not only for ^{39}Ar but also for ^{37}Ar and ^3H . Production rates
 520 from Ref. [35], based on a neutron irradiation experiment, have been con-
 521 sidered for the Ar isotopes while for ^3H an estimate of the production rate
 522 by cosmic neutrons made in this work obtaining (168 ± 53) atoms/kg/day
 523 has been used. The estimated cosmogenic activity of ^{39}Ar when all the UAr
 524 arrives to LNGS, (20.7 ± 2.8) $\mu\text{Bq}/\text{kg}$ for the assumed exposure history, is
 525 considered acceptable as it is just 2.8% of the residual activity measured
 526 in DarkSide-50 for UAr of the same source and would add ~ 1 Hz to the
 527 counting rate of the TPC. The quantified effect of some uncertain steps in
 528 the procedure of UAr production shows that there is enough contingency.
 529 Contributions from the induced activity of ^{37}Ar and ^3H are not problematic
 530 thanks to short half-life and purification, respectively. The results of this
 531 study of the cosmogenic activation of UAr will be useful to set exposure limi-
 532 tations for the procurement of the large amounts of radiopure UAr necessary
 533 in future LAr projects.

534 Acknowledgements

535 This report is based upon work supported by FSC 2014-2020 - Patto
 536 per lo Sviluppo, Regione Sardegna, Italy, the U. S. National Science Foun-
 537 dation (NSF) (Grants No. PHY-0919363, No. PHY-1004054, No. PHY-
 538 1004072, No. PHY-1242585, No. PHY-1314483, No. PHY- 1314507, as-
 539 sociated collaborative grants, No. PHY-1211308, No. PHY-1314501, and
 540 No. PHY-1455351, as well as Major Research Instrumentation Grant No.
 541 MRI-1429544), the Italian Istituto Nazionale di Fisica Nucleare (Grants
 542 from Italian Ministero dell'Istruzione, Università, e Ricerca Progetto Pre-

543 miale 2013 and Commissione Scientifica Nazionale II), the Natural Sciences
 544 and Engineering Research Council of Canada, SNOLAB, and the Arthur B.
 545 McDonald Canadian Astroparticle Physics Research Institute. We acknowl-
 546 edge the financial support by LabEx UnivEarthS (ANR-10-LABX-0023 and
 547 ANR18-IDEX-0001), the São Paulo Research Foundation (Grant FAPESP-
 548 2017/26238-4), Chinese Academy of Sciences (113111KYSB20210030) and
 549 National Natural Science Foundation of China (12020101004). The au-
 550 thors were also supported by the Spanish Ministry of Science and Inno-
 551 vation (MICINN) through the grant PID2019-109374GBI00, the “Atraccion
 552 de Talento” Grant 2018-T2/ TIC-10494, the Polish NCN, Grant No. UMO-
 553 2019/ 33/ B/ ST2/ 02884, the Polish Ministry of Science and Higher Ed-
 554 ucation, MNi-SW, grant number 6811/IA/SP/2018, the International Re-
 555 search Agenda Programme AstroCeNT, Grant No. MAB-/2018/7, funded by
 556 the Foundation for Polish Science from the European Regional Development
 557 Fund, the European Union’s Horizon 2020 research and innovation program
 558 under grant agreement No 952480 (DarkWave), the Science and Technology
 559 Facilities Council, part of the United Kingdom Research and Innovation,
 560 and The Royal Society (United Kingdom), and IN2P3-COPIN consortium
 561 (Grant No. 20-152). I.F.M.A is supported in part by Conselho Nacional
 562 de Desenvolvimento Científico e Tecnológico (CNPq). We also wish to ac-
 563 knowledge the support from Pacific Northwest National Laboratory, which is
 564 operated by Battelle for the U.S. Department of Energy under Contract No.
 565 DE-AC05-76RL01830. This research was supported by the Fermi National
 566 Accelerator Laboratory (Fermilab), a U.S. Department of Energy, Office of
 567 Science, HEP User Facility. Fermilab is managed by Fermi Research Alliance,
 568 LLC - (FRA), acting under Contract No. DE-AC02-07CH11359.

569 **References**

570 [1] G. Bertone and D. Hooper, History of dark matter, Rev. Mod. Phys. 90
 571 (2018) 045002, <https://doi.org/10.1103/RevModPhys.90.045002>.

572 [2] M. Schumann, Direct Detection of WIMP Dark Matter: Concepts and
 573 Status, J. Phys. G: Nucl. Part. Phys. 46 (2019) 103003, <https://doi.org/10.1088/1361-6471/ab2ea5>.

575 [3] J. Billard et al, Direct Detection of Dark Matter – APPEC Commit-
 576 tee Report, Rep. Prog. Phys. 85 (2022) 056201, <https://doi.org/10.1088/1361-6633/ac5754>.

578 [4] Y. Meng et al, Dark Matter Search Results from the PandaX-4T Com-
 579 missioning Run, Phys. Rev. Lett. 127 (2021) 261802, <https://doi.org/10.1103/PhysRevLett.127.261802>.

581 [5] E. Aprile et al (XENON Collaboration), Search for New Physics in Elec-
 582 tronic Recoil Data from XENONnT, Phys. Rev. Lett. 129 (2022) 161805,
 583 <https://doi.org/10.1103/PhysRevLett.129.161805>.

584 [6] J. Aalbers (LZ Collaboration), First Dark Matter Search Results from
 585 the LUX-ZEPLIN (LZ) Experiment, arXiv:2207.03764, <https://doi.org/10.48550/arXiv.2207.03764>.

587 [7] R. Ajaj et al (DEAP Collaboration), Search for dark matter with a
 588 231-day exposure of liquid argon using DEAP-3600 at SNOLAB, Phys.
 589 Rev. D 100 (2019) 022004, <https://doi.org/10.1103/PhysRevD.100.022004>.

591 [8] P. Agnes et al (The DarkSide Collaboration), DarkSide-50 532-day dark
 592 matter search with low-radioactivity argon, Phys. Rev. D 98 (2018)
 593 102006, <https://doi.org/10.1103/PhysRevD.98.102006>.

594 [9] P. Agnes et al (The DarkSide Collaboration), Low-Mass Dark Mat-
 595 ter Search with the DarkSide-50 Experiment, Phys. Rev. Lett. 121
 596 (2018) 08130, <https://doi.org/10.1103/PhysRevLett.121.081307>;
 597 Search for low-mass dark matter WIMPs with 12 ton-day exposure of
 598 DarkSide-50, Phys. Rev. D 107 (2023) 063001, <https://doi.org/10.1103/PhysRevD.107.063001>;
 599 Search for Dark-Matter–Nucleon Interac-
 600 tions via Migdal Effect with DarkSide-50, Phys. Rev. Lett. 130 (2023)
 601 101001, <https://doi.org/10.1103/PhysRevLett.130.101001>.

602 [10] P. Agnes et al (The DarkSide Collaboration), Constraints on Sub-
 603 GeV Dark-Matter Electron Scattering from the DarkSide-50 Experi-
 604 ment, Phys. Rev. Lett. 121 (2018) 111303, <https://doi.org/10.1103/PhysRevLett.121.111303>;
 605 Search for Dark Matter Particle Interac-
 606 tions with Electron Final States with DarkSide-50, Phys. Rev. Lett. 130
 607 (2023) 101002, <https://doi.org/10.1103/PhysRevLett.130.101002>.

608 [11] G. Heusser, Low-radioactivity background techniques, Annu. Rev. Nucl.
 609 Part. Sci. 45 (1995) 543, <https://doi.org/10.1146/annurev.ns.45.120195.002551>.

611 [12] J.A. Formaggio and C.J. Martoff, Backgrounds to sensitive experiments
 612 underground, *Annu. Rev. Nucl. Part. Sci.* 54 (2004) 361, <https://doi.org/10.1146/annurev.nucl.54.070103.181248>.

614 [13] S. Cebrián, Cosmogenic activation of materials, *Int. J. Mod. Phys. A* 32
 615 (2017) 1743006, <https://doi.org/10.1142/S0217751X17430060>.

616 [14] S. Cebrián, Cosmogenic Activation in Double Beta Decay Experiments,
 617 *Universe* 6 (2020) 162, <https://doi.org/10.3390/universe6100162>.

618 [15] I. Barabanov et al, Cosmogenic activation of germanium and its reduc-
 619 tion for low background experiments, *Nucl. Instrum. Meth. B* 251 (2006)
 620 115–120, <https://doi.org/10.1016/j.nimb.2006.05.011>.

621 [16] D. M. Mei et al, Cosmogenic production as a background in searching
 622 for Rare Physics processes, *Astropart. Phys.* 31 (2009) 417–420, <https://doi.org/10.1016/j.astropartphys.2009.04.004>.

624 [17] S. R. Elliott et al, Fast-neutron activation of long-lived isotopes in en-
 625 riched Ge, *Phys. Rev. C* 82 (2010) 054610, <https://doi.org/10.1103/PhysRevC.82.054610>.

627 [18] S. Cebrián et al, Cosmogenic activation in germanium and copper for
 628 rare event searches, *Astropart. Phys.* 33 (2010) 316–329, <https://doi.org/10.1016/j.astropartphys.2010.03.002>.

630 [19] E. Armengaud et al, Measurement of the cosmogenic activation of ger-
 631 manium detectors in EDELWEISS-III, *Astropart. Phys.* 91 (2017) 51–
 632 64, <https://doi.org/10.1016/j.astropartphys.2017.03.006>.

633 [20] J. Amaré et al, Cosmogenic production of tritium in dark matter detec-
 634 tors, *Astropart. Phys.* 97 (2018) 96–105, <https://doi.org/10.1016/j.astropartphys.2017.11.004>.

636 [21] R. Agnese et al, Production Rate Measurement of Tritium and Other
 637 Cosmogenic Isotopes in Germanium with CDMSlite, *Astropart. Phys.*
 638 104 (2019) 1–12, <https://doi.org/10.1016/j.astropartphys.2018.08.006>.

640 [22] J. L. Ma et al, Study on cosmogenic activation in germanium detectors
 641 for future tonne-scale CDEX experiment, *Science China-Physics, Mechanics and Astronomy* 62 (2019) 011011, <https://doi.org/10.1007/s11433-018-9215-0>.

644 [23] Y.L. Yan et al, Study on cosmogenic radioactive production in germanium as a background for future rare event search experiments, *Nucl. Sci. Tech.* 31 (2020) 55, <https://doi.org/10.1007/s41365-020-00762-1>.

647 [24] R. Saldanha et al, Cosmogenic activation of silicon, *Phys. Rev. D* 102 (2020) 102006, <https://doi.org/10.1103/PhysRevD.102.102006>.

649 [25] J. Amaré et al, Cosmogenic radionuclide production in NaI(Tl) crystals, *J. Cosm. Astrop. Phys.* 02 (2015) 046, <https://doi.org/10.1088/1475-7516/2015/02/046>.

652 [26] P. Villar et al, Study of the cosmogenic activation in NaI(Tl) crystals within the ANAIS experiment, *Int. J. Mod. Phys. A* 33 (2018) 1843006, <https://doi.org/10.1142/S0217751X18430066>.

655 [27] E. Barbosa de Souza et al, Study of cosmogenic radionuclides in the COSINE-100 NaI(Tl) detectors, *Astropart. Phys.* 115 (2020) 102390, <https://doi.org/10.1016/j.astropartphys.2019.102390>.

658 [28] R. Saldanha et al, Cosmogenic activation of sodium iodide, *Phys. Rev. D* 107 (2023) 022006, <https://doi.org/10.1103/PhysRevD.107.022006>.

660 [29] A. F. Barghouty et al, Measurements of p-induced radionuclide production cross sections to evaluate cosmic-ray activation of Te, *Nucl. Instrum. Meth. B* 295 (2013) 16–21, <https://doi.org/10.1016/j.nimb.2012.10.008>.

664 [30] V. Lozza and J. Petzoldt, Cosmogenic activation of a natural tellurium target, *Astropart. Phys.* 61 (2015) 62–71, <https://doi.org/10.1016/j.astropartphys.2014.06.008>.

667 [31] B.S. Wang et al, Cosmogenic-neutron activation of TeO₂ and implications for neutrinoless double-beta decay experiments, *Phys. Rev. C* 92 (2015) 024620, <https://doi.org/10.1103/PhysRevC.92.024620>.

670 [32] L. Baudis et al, Cosmogenic activation of xenon and copper,
 671 Eur. Phys. J. C 75 (2015) 485, <https://doi.org/10.1140/epjc/s10052-015-3711-3>.

673 [33] C. Zhang et al, Cosmogenic activation of materials used in rare event
 674 search experiments, Astropart. Phys. 84 (2016) 62–69, <https://doi.org/10.1016/j.astropartphys.2016.08.008>.

676 [34] J. Aalbers et al, Cosmogenic production of ^{37}Ar in the context of the
 677 LUX-ZEPLIN experiment, Phys. Rev. D 105 (2022) 082004, <https://doi.org/10.1103/PhysRevD.105.082004>.

679 [35] R. Saldanha et al, Cosmogenic production of ^{39}Ar and ^{37}Ar in argon,
 680 Phys. Rev. C 100 (2019) 024608, <https://doi.org/10.1103/PhysRevC.100.024608>.

682 [36] C. Zhang and D.M. Mei, Evaluation of cosmogenic production
 683 of ^{39}Ar and ^{42}Ar for rare-event physics using underground argon,
 684 Astropart. Phys. 142 (2022) 102733, <https://doi.org/10.1016/j.astropartphys.2022.102733>.

686 [37] W. Chen et al, Cosmogenic background study for a ^{100}Mo -based bolometric
 687 demonstration experiment at China JinPing underground Laboratory,
 688 Eur. Phys. J. C 82 (2022) 549, <https://doi.org/10.1140/epjc/s10052-022-10501-y>.

690 [38] M. Laubenstein, G. Heusser, Cosmogenic radionuclides in metals as indicator
 691 for sea level exposure history, App. Rad. Isot. 67 (2009) 750–754,
 692 <https://doi.org/10.1016/j.apradiso.2009.01.029>.

693 [39] Z. She et al, Study on cosmogenic activation in copper for rare event
 694 search experiments, Eur. Phys. J. C 81 (2021) 1041, <https://doi.org/10.1140/epjc/s10052-021-09827-w>.

696 [40] V.E. Guiseppe et al, Fast-neutron activation of long-lived nuclides in
 697 natural Pb, Astropart. Phys. 64 (2015) 34–39, <https://doi.org/10.1016/j.astropartphys.2014.11.002>.

699 [41] C. A. J. O'Hare, New Definition of the Neutrino Floor for Direct Dark
 700 Matter Searches, Phys. Rev. Lett. 127 (2021) 251802, <https://doi.org/10.1103/PhysRevLett.127.251802>.

702 [42] A. Gaspert et al, Neutrino backgrounds in future liquid noble element
 703 dark matter direct detection experiments, Phys. Rev. D 105 (2022)
 704 035020, <https://doi.org/10.1103/PhysRevD.105.035020>.

705 [43] P. Agnes et al, Sensitivity projections for a dual-phase argon TPC op-
 706 timized for light dark matter searches through the ionization channel,
 707 arXiv:2209.01177, <https://doi.org/10.48550/arXiv.2209.01177>.

708 [44] P. Agnes et al, Sensitivity of future liquid argon dark matter search
 709 experiments to core-collapse supernova neutrinos, JCAP 03 (2021) 043,
 710 <https://doi.org/10.1088/1475-7516/2021/03/043>.

711 [45] P. Agnes et al, Separating ^{39}Ar from ^{40}Ar by cryogenic distillation with
 712 Aria for dark-matter searches, Eur. Phys. J. C 81 (2021) 359, <https://doi.org/10.1140/epjc/s10052-021-09121-9>.

713 [46] E. Aaron et al, Measurement of isotopic separation of argon with
 714 the prototype of the cryogenic distillation plant Aria for dark mat-
 715 ter searches, accepted in Eur. Phys. J. C, arXiv:2301.09639, <https://doi.org/10.48550/arXiv.2301.09639>.

716 [47] C.E. Aalseth et al (The DarkSide-20k collaboration), Design and con-
 717 struction of a new detector to measure ultra-low radioactive-isotope con-
 718 tamination of argon, JINST 15 (2020) P02024, <https://doi.org/10.1088/1748-0221/15/02/P02024>.

719 [48] D. Akimov et al, First Measurement of Coherent Elastic Neutrino-
 720 Nucleus Scattering on Argon, Phys. Rev. Lett. 126 (2021) 012002,
 721 <https://doi.org/10.1103/PhysRevLett.126.012002>.

722 [49] N. Abgrall et al, The large enriched germanium experiment for neu-
 723 trinoless double beta decay (LEGEND), AIP Conf. Proc. 1894 (2017)
 724 020027

725 [50] E. Church, Ch. Jackson, R. Saldanha, Dark Matter Detection Capabil-
 726 ities of a Large Multipurpose Liquid Argon Time Projection Chamber,
 727 JINST 15 (2020) P092026, <https://doi.org/10.1088/1748-0221/15/09/P09026>.

732 [51] T. Alexander et al, The Low-Radioactivity Underground Argon Work-
 733 shop: A workshop synopsis, arXiv:1901.10108, <https://doi.org/10.48550/arXiv.1901.10108>.

735 [52] H. O. Back et al, A Facility for Low-Radioactivity Underground Argon,
 736 Snowmass2021 white Paper, arXiv:2203.09734, <https://doi.org/10.48550/arXiv.2203.09734>.

738 [53] P. Agnes et al, Direct Detection of Dark Matter with DarkSide-20k,
 739 EPJ Web of Conferences 280 (2023) 06003, <https://doi.org/10.1051/epjconf/202328006003>.

741 [54] P. Agnes et al, Simulation of argon response and light detection in the
 742 DarkSide-50 dual phase TPC, JINST 12 (2017) P10015, <https://doi.org/10.1088/1748-0221/12/10/P10015>.

744 [55] M. S. Gordon et al, Measurement of the Flux and Energy Spectrum of
 745 Cosmic-Ray Induced Neutrons on the Ground, IEEE Trans. Nucl. Sci. 51
 746 (2004) 3427–3434, <https://doi.org/10.1109/TNS.2004.839134>. Erratum: M. S. Gordon et al, IEEE Transactions on Nuclear Science 52
 747 (2005) 2703.

749 [56] J.F. Ziegler, Terrestrial cosmic ray intensities, IBM J. Res. Dev. 42
 750 (1998) 117, <https://doi.org/10.1147/rd.421.0117>.

751 [57] N. Otuka et al, Towards a More Complete and Accurate Experimental
 752 Nuclear Reaction Data Library (EXFOR): International Collaboration
 753 Between Nuclear Reaction Data Centres (NRDC), Nucl. Data Sheets
 754 120 (2014) 272, <https://doi.org/10.1016/j.nds.2014.07.065>.

755 [58] R. Silberberg and C. H. Tsao, Partial Cross-Sections in High-Energy Nu-
 756 clear Reactions, and Astrophysical Applications. I. Targets With $z \leq 28$,
 757 Astrophys. J. Suppl. Ser. 25 (1973) 315; ibid p. 335.

758 [59] R. Silberberg and C. H. Tsao, Cross sections for (p, xn) reactions, and
 759 astrophysical applications, Astrophys. J. Suppl. Ser. 35 (1977) 129; Im-
 760 proved cross section calculations for astrophysical applications, Astro-
 761 phys. J. Suppl. Ser. 58 (1985) 873; Spallation processes and nuclear
 762 interaction products of cosmic rays, Phys. Rep. 191 (1990) 351.

763 [60] R. Silberberg and C. H. Tsao, Updated partial cross sections of proton-
 764 nucleus reactions, *Astrophys. J.* 501 (1998) 911, <https://doi.org/10.1086/305862>.

766 [61] J. Martoff and P.D. Lewin, COSMO- a program to estimate spalla-
 767 tion radioactivity produced in a pure substance by exposure to cosmic-
 768 radiation on the Earth, *Comput. Phys. Commun.* 72 (1992) 96, [https://doi.org/10.1016/0010-4655\(92\)90008-M](https://doi.org/10.1016/0010-4655(92)90008-M).

770 [62] J.J. Back, Y.A. Ramachers, ACTIVIA: Calculation of isotope produc-
 771 tion cross-sections and yields, *Nucl. Instrum. Meth. A* 586 (2008) 286-
 772 294, <https://doi.org/10.1016/j.nima.2007.12.008>.

773 [63] A. J. Koning et al, TENDL: Complete Nuclear Data Library for Inno-
 774 vative Nuclear Science and Technology, *Nucl. Data Sheets* 155 (2019) 1,
 775 <https://doi.org/10.1016/j.nds.2019.01.002>.

776 [64] K. Shibata et al, JENDL-4.0: A New Library for Nuclear Science and
 777 Engineering, *J. Nucl. Sci. Technol.* 48 (2011) 1, <https://doi.org/10.1080/18811248.2011.9711805>.

779 [65] Y. A. Korovin et al, High Energy Activation Data Library (HEAD-
 780 2009), *Nucl. Instrum. Meth. A* 624 (2010) 20-26, <https://doi.org/10.1016/j.nima.2010.08.110>.

782 [66] Decay Data Evaluation Project, http://www.lnhb.fr/ddep_wg/

783 [67] The Lund/LBNL Nuclear Data Search, <http://nucleardata.nuclear.lu.se/toi>.

785 [68] P. Benetti et al, Measurement of the specific activity of ^{39}Ar in natural
 786 argon, *Nucl. Instrum. Meth. A* 574 (2007) 83, <https://doi.org/10.1016/j.nima.2007.01.106>.

788 [69] J. Calvo et al, Backgrounds and pulse shape discrimination in the ArDM
 789 liquid argon TPC, *JCAP* 12 (2018) 011, <https://doi.org/10.1088/1475-7516/2018/12/011>.

791 [70] R. Ajaj et al (DEAP Collaboration), Electromagnetic Backgrounds and
 792 Potassium-42 Activity in the DEAP-3600 Dark Matter Detector, *Phys.*
 793 *Rev. D* 100 (2019) 072009, <https://doi.org/10.1103/PhysRevD.100.072009>.

795 [71] P. Agnes et al (DarkSide Collaboration), Results from the first use of
 796 low radioactivity argon in a dark matter search, Phys. Rev. D 93 (2016)
 797 081101(R), <https://doi.org/10.1103/PhysRevD.93.081101>.

798 [72] A. Lubashevskiy et al, Mitigation of $^{42}\text{Ar}/^{42}\text{K}$ background for the
 799 GERDA Phase II experiment, Eur. Phys. J. C 78 (2018) 15, <https://doi.org/10.1140/epjc/s10052-017-5499-9>.

800 [73] P. Cennini et al, On atmospheric ^{39}Ar and ^{42}Ar abundance, Nucl. Inst.
 801 Meth. A 356 (1995) 526, [https://doi.org/10.1016/0168-9002\(94\)01234-2](https://doi.org/10.1016/0168-9002(94)01234-2).

802 [74] A.S. Barabash, R.R. Saakyan, V.I. Umatov, On concentration of ^{42}Ar
 803 in liquid argon, J. Phys.: Conf. Ser. 718 (2016) 062004, <https://doi.org/10.1088/1742-6596/718/6/062004>.

804 [75] J. Amaré et al, Analysis of backgrounds for the ANAIS-112 dark matter
 805 experiment, Eur. Phys. J. C 79 (2019) 412, <https://doi.org/10.1140/epjc/s10052-019-6911-4>.

806 [76] P. Adhikari et al, Background model for the NaI(Tl) crystals in
 807 COSINE-100, Eur. Phys. J. C 78 (2018) 490, <https://doi.org/10.1140/epjc/s10052-018-5970-2>.

808 [77] E. Aprile et al (XENON Collaboration), Observation of Excess Elec-
 809 tronic Recoil Events in XENON1T, Phys. Rev. D 102 (2020) 072004,
 810 <https://doi.org/10.1103/PhysRevD.102.072004>.

811 [78] A.E. Robinson, XENON1T observes tritium, arXiv:2006.13278, <https://doi.org/10.48550/arXiv.2006.13278>.

812 [79] D. H. Meikrantz et al, Tritium Process Applications Using SAES Getters
 813 for Purification and Collection from Inert Gas Streams, Fus. Technol.
 814 27 (1995) 14, <https://doi.org/10.13182/FST95-A11963799>.

815 [80] S. MacMullin et al, Partial γ -ray production cross sections for $(\text{n},\text{xn}\gamma)$
 816 reactions in natural argon at 1-30 MeV, Phys. Rev. C 85 (2012) 064614,
 817 <https://doi.org/10.1103/PhysRevC.85.064614>.

818 [81] S. M. Qaim, R. Wolfle, Triton emission in the interactions of fast neu-
 819 trons with nuclei, Nucl. Phys. A 295 (1978) 150–162, [https://doi.org/10.1016/0375-9474\(78\)90026-X](https://doi.org/10.1016/0375-9474(78)90026-X).

820

821

822

823

824

825

826

Declaration of interests

The authors declare that they have no known competing financial interests or personal relationships that could have appeared to influence the work reported in this paper.

The authors declare the following financial interests/personal relationships which may be considered as potential competing interests: